Draft version January 5, 2020
Typeset using LaTeX **preprint** style in AASTeX62

N-body simulations of the Self–Confinement of Viscous Self–Gravitating Narrow Eccentric Planetary Ringlets

Joseph M. Hahn,[1] Douglas P. Hamilton,[2] Thomas Rimlinger,[2] and Lucy Luu[2]

[1] *Space Science Institute*
[2] *University of Maryland*

(Received not yet; Revised not yet; Accepted not yet)

Submitted to Somewhere, eventually

ABSTRACT

The following uses a suite of N-body simulations to illustrate how narrow eccentric planetary ringlets can evolve into a self–confining state.

Keywords: editorials, notices — miscellaneous — catalogs — surveys — update, me

1. INTRODUCTION

Narrow eccentric planetary ringlets have properties both interesting and not well understood: sharp edges, sizable eccentricity gradients, and a confinement mechanism that opposes radial spreading due to ring viscosity. Prevailing ringlet confinement mechanisms include: unseen shepherd satellites (reference), periapse pinch (ref), self gravity (ref), and self-confinement (ref). This study uses N-body simulations to show how narrow self–gravitating ringlets can evolve into a self-confining state.

2. RINGLET CONFINEMENT MECHANISMS

This section will explain the pros and cons of the various ringlet confinement mechanisms, and then motivates the possibility that ringlets are self confining. That possibility is explored further via numerical simulations using the epi_int_lite N-body integrator.

3. EPI_INT_LITE

Epi_int_lite is a child of the epi_int N-body integrator that was used to simulate the outer edge of Saturn's B ring as it is sculpted by satellite perturbations (Hahn & Spitale 2013). The new code is very similar to its parent but differs in three significant ways: (*i.*) epi_int_lite is written in python and recoded for more efficient execution, (*ii.*) epi_int_lite uses a more accurate drift step for unperturbed motion around an oblate planet (detailed in Appendix A), and (*iii.*) epi_int_lite uses the $C = 1$ approximation that is justified below (Appendix B).

Otherwise epi_int_lite's treatment of ring self–gravity and viscosity are identical to that used by the parent code; see Hahn & Spitale (2013) for additional details. The epi_int_lite source code is available

Corresponding author: Joseph M. Hahn
jhahn@spacescience.org

at https://github.com/joehahn/epi_int_lite, and the code's numerical quality is assessed in Appendix C where the output of several numerical experiments are compared against theoretical predictions.

Calculations performed by epi_int_lite use natural units with gravitation constant $G = 1$, central primary mass $M = 1$, and the ringlet's inner edge has initial radius $r_0 = 1$, and so the ringlet masses m_r and radii r quoted below are in units of M and r_0. Converting code output from natural units to physical units requires choosing physical values for M and r_0 and multiplying accordingly, and when this text does so it assumes Saturn's mass $M = 5.68 \times 10^{29}$ gm and a characteristic ring radius $r_0 = 1.0 \times 10^{10}$ cm. Simulation time t is in units of $T_{\rm orb}/2\pi$ where $T_{\rm orb} = 2\pi\sqrt{r_0^3/GM}$ is the orbit period at r_0, so dividing t by 2π and then multiplying by $T_{\rm orb}$ converts simulation time from natural to physical units. The simulated particles' motions during the drift step are also sensitive to the J_2 portion of the primary's non-spherical gravity component (see Appendix B), and all simulations adopt a Saturn-like value of $J_2 = 0.01$ and $R_p = r_0/2$ where R_p is the planet's mean radius.

Initially all particles are assigned to various streamlines across the simulated ringlet. A streamline is a closed eccentric path around the primary, and the N_p particles in a given streamline are initially assigned a common semimajor axis a and eccentricity e, with uniform spacing in longitude. Most of the simulations described below employ only $N_s = 2$ streamlines, so that the model output can be benchmarked against theoretical treatments that also treat the ringlet as two gravitating rings (e.g. Borderies et al. 1983). But the following also performs a few higher-resolution simulations using $N_s = 11$ streamlines, to demonstrate that the $N_s = 2$ treatment appears perfectly adequate and reproduces all the relevant dynamics. All simulations use $N_p = 241$ particles per streamline, and the total number of particles is $N_s N_p$. Note that the assignment of particles to a given streamline is merely for labeling purposes, as particles are still free to wander in response to the ring's internal forces, namely, ring gravity and viscosity. But as Hahn & Spitale (2013) as well as this work shows, the simulated ring stays coherent and highly organized throughout the simulation such that particles on the same streamline do not pass each other longitudinally, nor do they cross adjacent streamlines. Because the simulated ringlet stays highly organized, there is no radial or longitudinal mixing of the ring particles, and simulated particles preserve their streamline membership over time.

4. N-BODY SIMULATIONS OF VISCOUS GRAVITATING RINGLETS

This Section describes a suite of N-body simulations of narrow viscous gravitating planetary ringlets, to highlight the range of initial ringlet conditions the do evolve into a self-confining state, and those that do not.

4.1. *nominal model*

Figure 1 shows the semimajor axis evolution of what is referred to as the nominal model since this ringlet readily evolves into a self-confining state. The simulated ringlet is composed of $N_s = 2$ streamlines having $N_p = 241$ particles per streamline, and the integrator timestep is $\Delta t = 0.5$ in natural units, so the integrator samples the particles' orbits $2\pi/\Delta t \simeq 13$ times per orbit, and this ringlet is evolved for 6.7×10^5 orbits, which requires 40 minutes execution time on a 5 year old laptop. The ringlet's mass is $m_r = 2 \times 10^{-9}$, its shear viscosity is $\nu_s = 1 \times 10^{-12}$, and its bulk viscosity is $\nu_b = 1.5\nu_s$. The ringet's initial radial width is $\Delta a_0 = 5 \times 10^{-4}$, its initial eccentricity is $e = 0.03$, and its eccentricity gradient is initially zero. A convenient measure of time is the ringlet's viscous radial spreading timescale

$$\tau_\nu = \frac{\Delta a_0^2}{12\nu_s}, \tag{1}$$

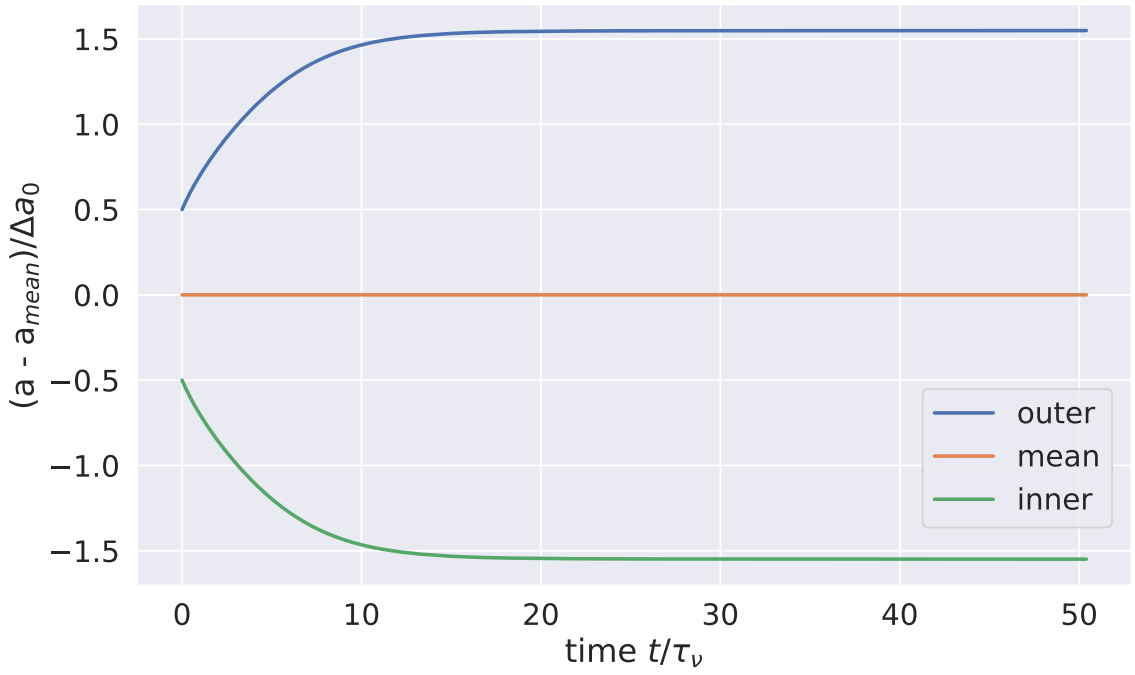

Figure 1. Evolution of the nominal ringlet's semimajor axes a versus time t in units of the ringlet's viscous time τ_ν. This ringlet is composed of $N_s = 2$ streamlines, and the outer (blue) and inner (green) streamlines' semimajor axes are plotted relative to their mean $a_{\rm mean}$, and displayed in units of the ringlet's initial width $\Delta a_0 = 5 \times 10^{-4}$ in natural units (*i.e.* $G = M = r_0 = 1$). The simulated ringlet has total mass $m_r = 2 \times 10^{-9}$, shear viscosity $\nu_s = 1 \times 10^{-12}$, and initial eccentricity $e = 0.03$. See Section 4.1 to convert m_r, a and ν_s from natural units to physical units.

which can be inferred from Eqn. (2.13) of Pringle (1981). This simulation's viscous timescale is $\tau_\nu = 2.1 \times 10^4$ in natural units or $\tau_\nu/2\pi = 3.3 \times 10^3$ orbital periods. If this ringlet were orbiting Saturn at $r_0 = 1.0 \times 10^{10}$ cm then the simulated ringlet's physical mass would be $m_r = 1.1 \times 10^{21}$ gm which is equivalent to a 64 km radius iceball assuming a volume density $\rho = 1$ gm/cm^3, and the ringlet's initial radial width would be $\Delta a_0 = 5 \times 10^{-4} r_0 = 50$ km. This ringlet's orbit period would be $T_{orb} = 2\pi\sqrt{r_0^3/GM} = 9.0$ hours in physical units, so the ringlet's viscous timescale is $\tau_\nu = 3.4$ years which indicates that shear viscosity is $\nu_s = \Delta a_0^2/12\tau_\nu = 1.9 \times 10^4$ cm^2/sec when evaluated in physical units. This ringlet's initial surface density would be $\sigma = m_r/2\pi r_0 \Delta a_0 = 3500$ gm/cm^2, but Figs. 1–2 show that shrinks by a factor of 3 as the ringlet's sememajor axis width Δa grows via viscous spreading until it settles into the anticipated self-confining state at time $t \sim 15\tau_\nu$. So the so-called nominal ringlet is probably overdense and overly viscous compared to known planetary ringlets, but that is by design so that the simulated ringlet quickly settles into the self-confining state. Section XX also shows how outcomes scale when a wide variety of alternate initial masses, orbits, and viscosities are also considered.

Figure 3 shows that the outer streamline's eccentricity grows at the expense of the inner streamline's, and this is a consequence the self-gravitating ringlet's secular perturbations of itself, which is also demonstrated in Appendix D. Figure 4 shows the ringlet's eccentricity difference $\Delta e = e_{\rm outer} - e_{\rm inner}$ and longitude of periapse difference $\Delta\tilde{\omega} = \tilde{\omega}_{\rm outer} - \tilde{\omega}_{\rm inner}$, which both settle into equilibrium values when the ringlet arrives in the self-confining state. It is convenient to recast these orbit element

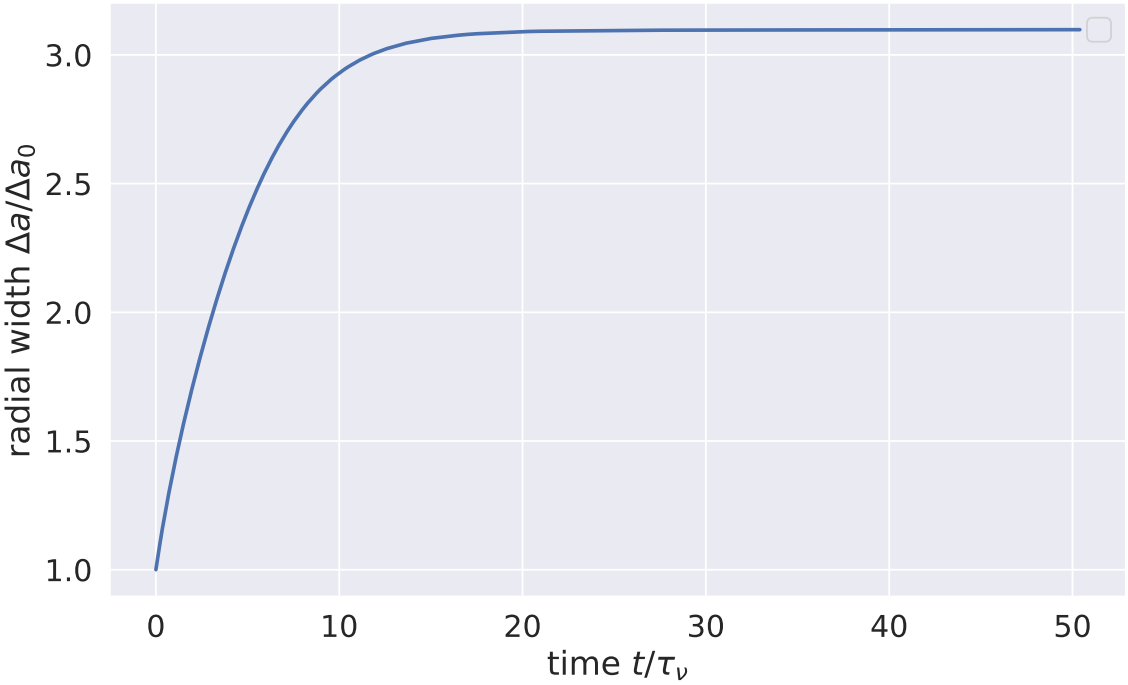

Figure 2. The nominal ringlet's semimajor axis width $\Delta a = a_{\rm outer} - a_{\rm inner}$ over time, in units of its initial radial width Δa_0.

differences as dimensionless gradients

$$e' = a\frac{de}{da} \qquad \text{and} \qquad \tilde{\omega}' = ea\frac{d\tilde{\omega}}{da} \tag{2}$$

as both terms contribute to the nonlinearity parameter of Borderies et al. (1983):

$$q = \sqrt{e'^2 + \tilde{\omega}'^2}. \tag{3}$$

See also Fig. 5 which plot's the nominal ringlet's dimensionless eccentricity gradient e', dimensionless periapse twist $\tilde{\omega}'$ and nonlinearity parameter q versus time. All simulations examined here have $|\tilde{\omega}'| \ll |e'|$ so that $q \simeq |e'|$, and all simulated self-confining ringlets have a positive eccenticity gradient and a negative periapse twist such that the outer ringlet's periapse trails the inner ringlet's, consistent with the findings of Borderies et al. (1983).

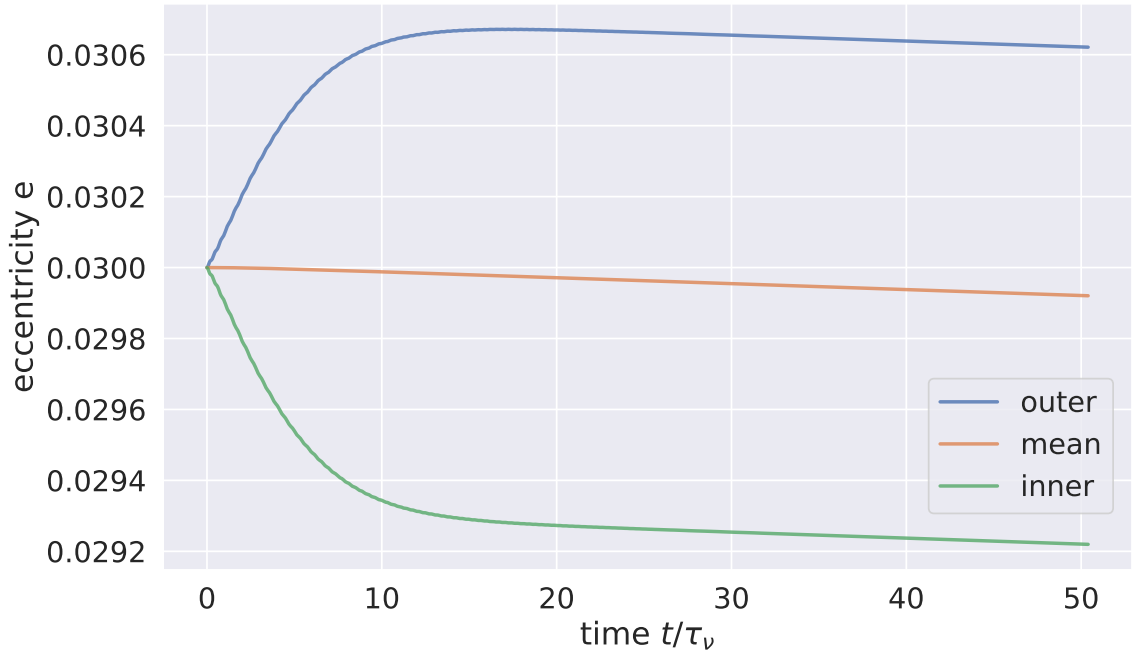

Figure 3. The nominal ringlet's eccentricity evolution.

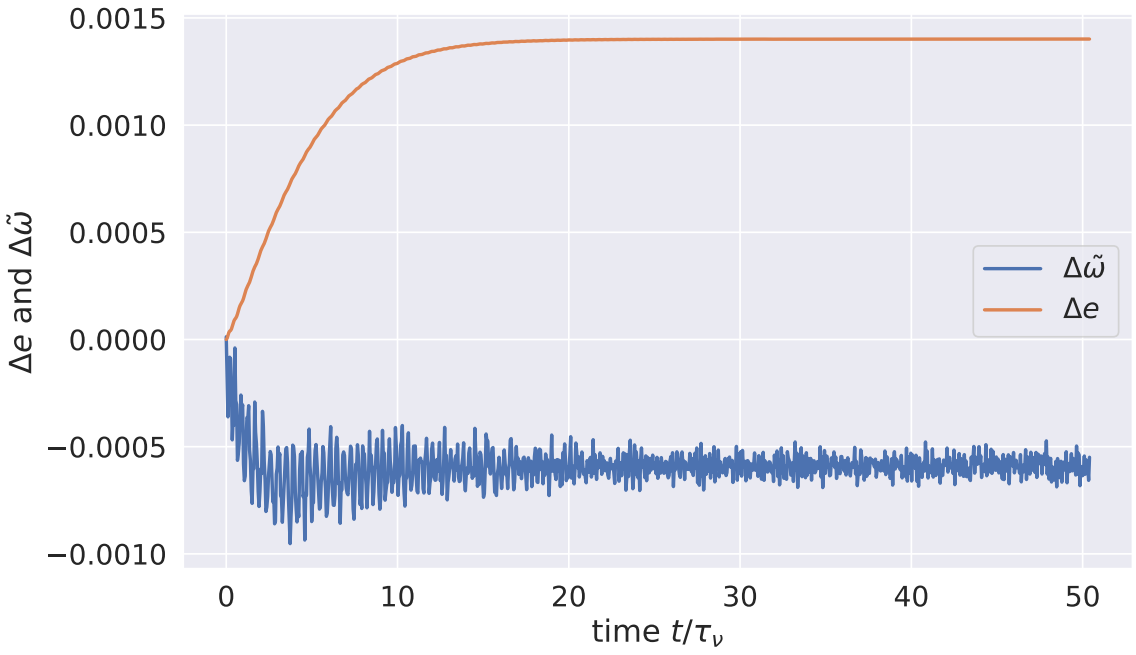

Figure 4. The nominal ringlet's eccentricity difference $\Delta e = e_{\text{outer}} - e_{\text{inner}}$ and longitude of periapse difference $\Delta\tilde{\omega} = \tilde{\omega}_{\text{outer}} - \tilde{\omega}_{\text{inner}}$.

Borderies et al. (1982) examine angular momentum transport in a viscous eccentric non-gravitating ringlet, and show that that transport has three noteworthy regimes that are distinguished by the ringlet's q:

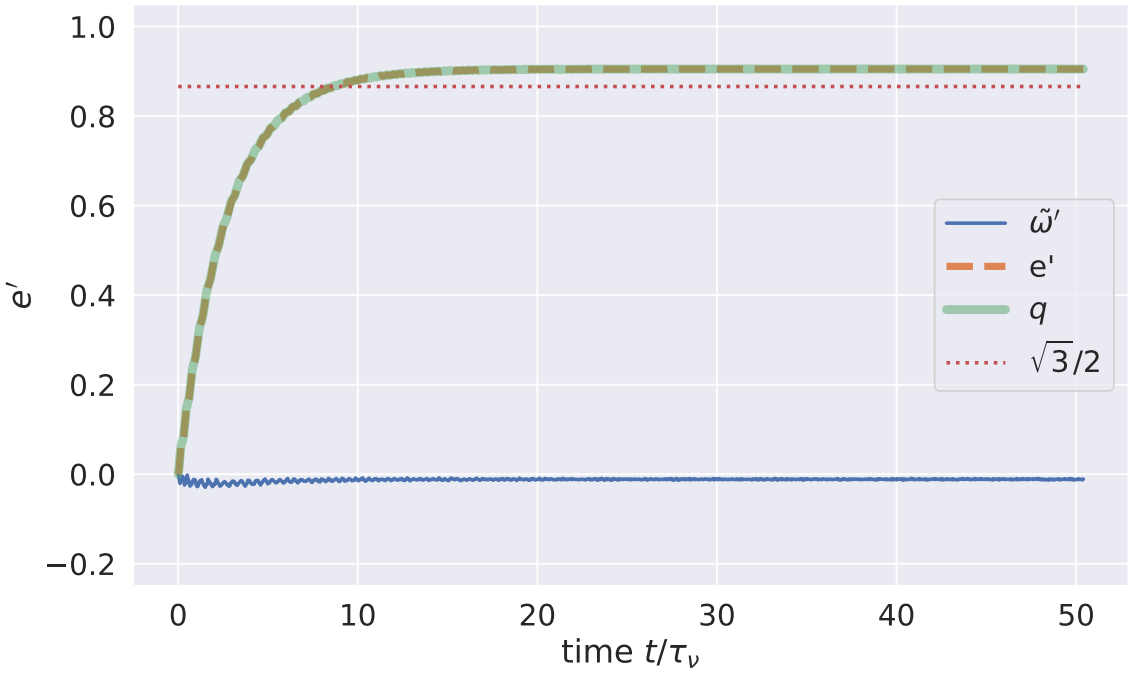

Figure 5. The nominal ringlet's dimensionless eccentricity gradient $e' = a\Delta e/\Delta a$ (dashed orange curve), dimensionless periapse twist $\tilde{\omega}' = ea\Delta\tilde{\omega}/\Delta a$ (blue curve), and nonlinearity parameter $q = \sqrt{e'^2 + \tilde{\omega}'^2}$ (green curve) versus time t/τ_ν. Dotted red curve has $e' = \sqrt{3}/2 \simeq 0.866$ and is the threshold for self-confinement in a non-gravitating ringlet.

1. $q < 3/4$. In this case the ringlet's viscous angular momentum flux $F_\nu(\theta) > 0$ at all ringlet longitudes θ. F_ν integrated over all ringlet longitudes is the ringlet's viscous angular momentum luminosity, $L_\nu = \oint F_\nu(\theta) d\ell > 0$, and $L_\nu > 0$ when $q < 0.75$. Viscous friction transports angular momentum radially outwards, so inner ring matter evolves to smaller orbits while exterior ring matter evolves outwards, and the ringlet spreads radially.

2. $3/4 < q < \sqrt{3}/4$. In this regime there is a range of longitudes θ where the viscous angular momentum flux is reversed such that $F_\nu(\theta) < 0$. Nonetheless L_ν, which is proportional to the orbit-average of $F_\nu(\theta)$, is positive and the ringlet spreads radially, albeit slower than when $q < 0.75$.

3. $q \geq \sqrt{3}/4$. Viscous angular momentum flux reversal is complete, $L_\nu < 0$, viscous friction transports angular momentum radially inwards, and the ringlet shrinks radially. But if $q = \sqrt{3}/4 \simeq 0.866$ then $L_\nu = 0$ and the ringlet's radial evolution ceases, the ringlet is self confining.

Note though that the nominal ringlet's eccentricity gradient $e' \simeq q$ exceeds the $q = \sqrt{3}/4 \simeq 0.866$ threshold (which is the dotted red line in Fig. 5) when it settles into self-confinement. The following shows that this is due to the ringlet's self-gravity, which also transports angular momentum radially through the ringlet.

The viscous flux of angular momentum is (Pringle?)

$$F_\nu(r, \theta) = -\nu_s \sigma r^2 \frac{\partial \omega}{\partial r} \tag{4}$$

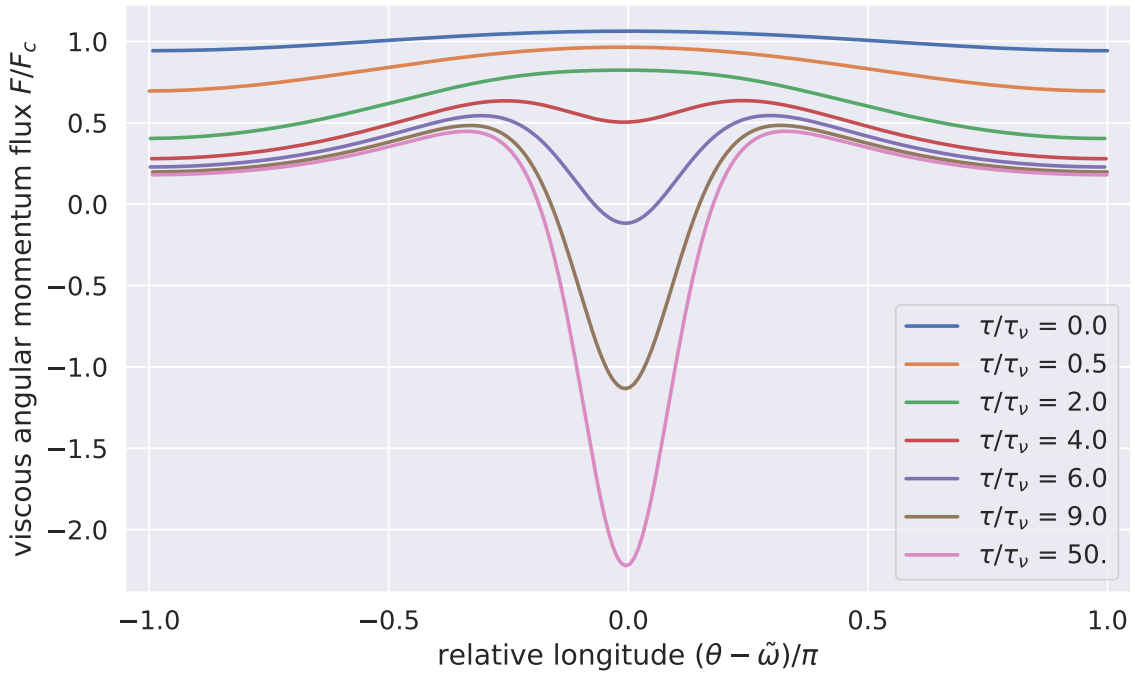

Figure 6. yadda yadda yadda.

where $\omega = \dot{\theta}$ is the angular velocity, Eqn. (XX). Figure 6 plots F_ν versus relative longitude $\varphi = \theta - \tilde{\omega}$ for the nominal ringlet at selected times t.

$$F_\nu(a, \varphi) = F_{\nu,0} \frac{1 - \frac{4}{3} e' \cos\varphi}{(1 - e' \cos\varphi)^2} \tag{5}$$

This research was supported by the National Science Foundation via Grant No. AST-1313013.

APPENDIX

A. APPENDIX A

Derive the more accurate drift step used by epi_int_lite...

B. APPENDIX B

Detail the $C = 1$ approximation used by epi_int_lite, and show that the errors associated with this approximation are negligible...

C. APPENDIX C

Compare epi_int_lite to theoretical predictions

D. APPENDIX D

This examines the viscous evolution of a narrow eccentric non-gravitating ringlet that is identical to the nominal ringlet of Section 4.1 but with ringlet self-gravity neglected and $J_2 = 0$. As the orange curve in Fig. 7 shows, the non-gravitating ringlet's radial width Δa grows steadily over time due

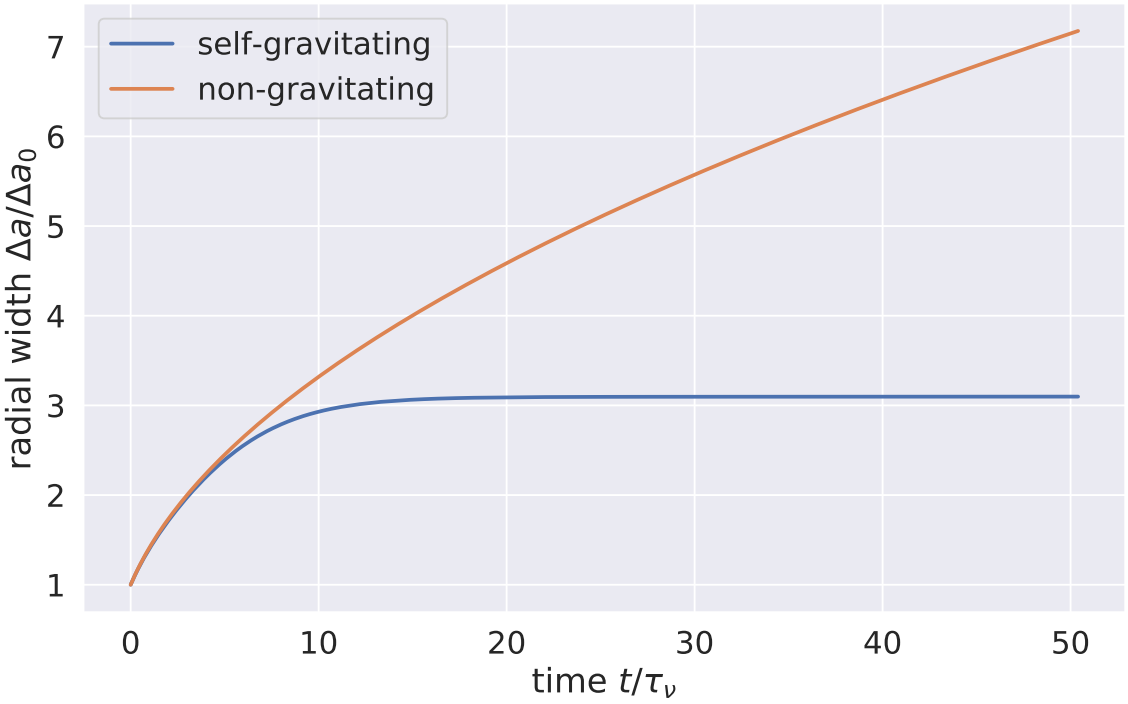

Figure 7. Blue curve is the nominal ringlet's semimajor axis width Δa versus time t, and this ringlet's radial spreading ceases by time $t \sim 15\tau_\nu$ when it's self-gravity has excited the ringlet's eccentricity gradient e' sufficiently; see blue curve in Fig. 8. Orange curve shows that the non-gravitating ringlet's Δa grows without limit due to the ringlet's much lower eccentricity gradient. Note that planetary oblateness would cause the non-gravitating streamlines to precess differentially and eventually cross when $J_s > 0$, so the non-gravitating simulation also sets $J_2 = 0$ to avoid differential precession.

to ringlet viscosity, long after the nominal self-gravitating ringlet (blue curve) has settled into the self-confining state by time $t \sim 15\tau_\nu$. This is due to the ringlet's secular gravitational perturbations of itself, which tends to excites the ringlet's outer streamline's eccentricity at the expense of the inner streamline (see Fig. 3) until the ringlet eccentricity gradient e' (blue curve in Fig. 8) grows beyond the limit required for complete angular momentum flux reversal that results in the ringlet's radial confinement (dotted line). Note that viscosity also excites the non-gravitating ringlet's eccentricity gradient some (orange curve), but insufficient to halt the ringlet's viscous spreading.

E. APPENDIX E

This Appendix will use the orbit elements derived in Appendix A to derive Eqn. 5 from 4.

For circular orbits

$$F_{\nu,0} = \frac{3}{2}\nu_s \sigma_0 a \Omega \tag{E1}$$

REFERENCES

Borderies, N., Goldreich, P., & Tremaine, S. 1982, Nature, 299, 209
—. 1983, Icarus, 55, 124
Hahn, J. M., & Spitale, J. N. 2013, ApJ, 772, 122
Pringle, J. E. 1981, ARA&A, 19, 137

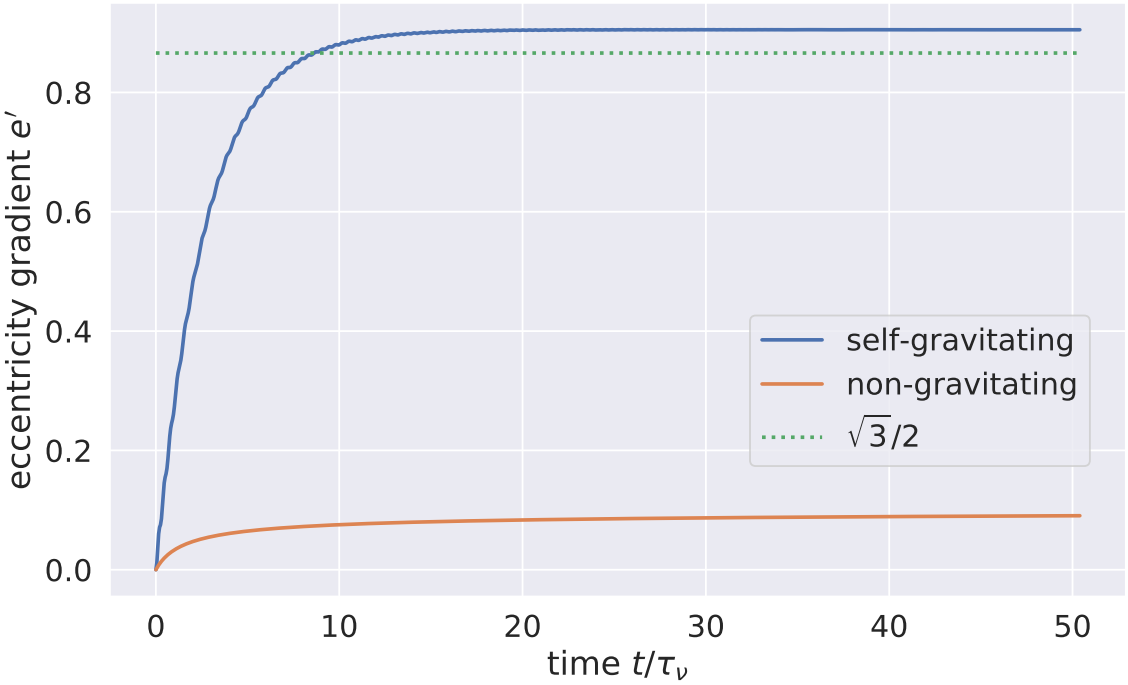

Figure 8. blah